Optimal estimation of cloud properties from thermal infrared observations with a combination of deep learning and radiative transfer simulation

He Huang[1], Quan Wang[1], Chao Liu[2], Chen Zhou[1]

[1] School of Atmospheric Sciences, Nanjing University, Nanjing, 210023, China

[2] Collaborative Innovation Center on Forecast and Evaluation of Meteorological Disasters, Nanjing University of Information Science and Technology, Nanjing, 210044, China

Correspondence to: Chen Zhou (czhou17@nju.edu.cn)

Abstract. While traditional thermal infrared retrieval algorithms based on radiative transfer models (RTM) could not effectively retrieve the cloud optical thickness of thick clouds, machine learning based algorithms were found to be able to provide reasonable estimations for both daytime and nighttime. Nevertheless, stand-alone machine learning algorithms are occasionally criticized for the lack of explicit physical processes. In this study, RTM simulations and a machine learning algorithm are synergistically utilized using the optimal estimation (OE) method to retrieve cloud properties from thermal infrared radiometry measured by Moderate Resolution Imaging Spectroradiometer (MODIS). In the new algorithm, retrievals from a machine learning algorithm are used to provide a priori states for the iterative process of OE method, and an RTM is used to create radiance lookup tables that are used in the iteration processes. Compared with stand-alone OE, the cloud properties retrieved by the new algorithm show an overall better performance by using statistic a priori information obtained by machine learning algorithm. Compared with stand-alone machine-learning based algorithm, the radiances simulated based on retrievals from the new method align more closely with observations, and physical radiative processes are handled explicitly in the new algorithm. Therefore, the new method combines the advantages of RTM-based cloud retrieval methods and machine-learning models. These findings highlight the potential for machine-learning-based algorithms to enhance the efficacy of conventional remote sensing techniques.

1 Introduction

Clouds play an important role in the Earth's energy budget by altering radiation patterns at both the surface and the top of the atmosphere (TOA) (Liou and Davies, 1993; Stubenrauch et al., 2006). Cloud

properties change in response to variations in greenhouse gases, aerosol concentrations, and global

30   surface temperature, leading to large uncertainties in climate change projections (Forster et al., 2021; Sassen et al., 2007). Grasping the variations in cloud properties is crucial for a comprehensive understanding of cloud dynamics and their radiative impacts on global climate change. The advancement of science and technology has positioned satellite remote sensing as a pivotal tool for monitoring cloud behaviors across diverse spatial and temporal scales. Active satellites like CloudSat and CALIPSO

35   (Cloud-Aerosol Lidar and Infrared Pathfinder Satellite Observations) offer unparalleled cloud profiling capabilities (Marchand et al., 2008; Sassen et al., 2009). Conversely passive satellites, known for their extensive swath observations, are widely applied in a range of atmospheric research.

In recent decades, numerous efforts have been made to retrieve cloud properties using passive satellite instruments (Lai et al., 2019; Li et al.,2023; Min et al., 2020; Minnis et al., 2011; Poulsen et al.,

40   2012; Tan et al., 2022; Zhao et al., 2012). A common method involves combining data from visible (VIS) and near-infrared (NIR) channels to construct lookup tables (LUT) for daytime cloud microphysical properties, such as cloud optical thickness (COT) and cloud effective radius (CER) (Painemal and Zuidema, 2011; Twomey et al., 1980; Nakajima et al., 1990). This approach is grounded in the principle that cloud reflectance in non-absorbing VIS wavelengths predominantly depends on COT, while

45   reflectance in absorbing NIR wavelengths is closely related to cloud effective radius (Arking and Childs, 1985; Rossow et al., 1989). Additionally, distinguishing liquid water from ice clouds using NIR channels (e.g., 1.65 μm) has also proven beneficial for deriving cloud top height (CTH) (Harshvardhan et al., 2009; Menzel et al., 2008; Pilewskie et al., 1987). Nonetheless, these VIS/NIR-based methodologies are confined to daytime operations owing to their reliance on incident solar radiation, absent during nighttime

50   hours.

Alternatively, night-time cloud properties can be retrieved using thermal infrared (TIR) radiometry from passive satellite. Inoue (1985) employed the split-window method, leveraging brightness temperature (BT) and BT differences across various window channels, to derive COT and CER. Subsequently, numerous improvements and enhancements have been made to this method (Hamada and

55   Nishi, 2010; Iwabuchi et al., 2018; Yang et al., 2005). Wang et al. (2016a) implemented an optimal estimation-based (OE) algorithm with Moderate Resolution Imaging Spectroradiometer (MODIS) infrared (IR) observations for cloud property retrieval, demonstrating the suitability of IR channels for

thin ice cloud properties during both daytime and nighttime (Wang et al., 2016b). In addition, the CO_2-slicing method, which utilizes channels with a wavelength between 13-15 μm, is able to retrieve CTH

60 effectively (Smith et al., 1974; Menzel et al., 1983). The atmospheric window IR measurements are also useful for CTH determination by comparing with the ambient atmospheric temperature profile (Garrett et al., 2009; Hong et al., 2007). However, IR window methods are less effective for optically thick clouds as their BT approaches asymptotic values (Garrett et al., 2009; Iwabuchi et al., 2016). While far infrared channels (>15 μm) are useful for ice clouds with substantial optical thickness (Libois et al., 2017), these

65 far infrared channels are rarely measured by satellites during the last decade. Moreover, the retrieval methods based on plane-parallel cloud radiative transfer (RT) models face global application challenges due to their high computational demands (Wang et al., 2013).

Recently, machine learning techniques such as random forests, artificial neural network, and deep learning have gained significant traction in remote sensing (Bai et al., 2021; Guo et al. 2022; Shi et

70 al.,2020; Tan et al.,2023; Yuan et al., 2020; Zhao et al., 2023). Häkansson et al. (2018) used a neural network algorithm to retrieve cloud top properties from several passive polar orbit sensors, greatly improving CTH retrievals. Advanced machine learning algorithms have particularly enhanced CTH retrievals for high and thin clouds (Min et al., 2020). Wang et al. (2022) developed a convolutional neural network (CNN)-based framework (TIR-CNN), which utilizes TIR radiometry from MODIS to retrieve

75 COT, CER, and CTH. This framework demonstrates well consistent with both passive and active cloud products and is effective during both daytime and nighttime (Wang et al., 2022, 2023). Tana et al. (2023) obtained cloud detection and cloud microphysical properties with high spatial-temporal resolutions from TIR spectral channels of Himawari-8 using a machine learning algorithm. Zhao et al. (2023) applied a deep-learning ResUnet model for retrieving cloud phase (CLP), COT, CER, and CTH using Fengyun-

80 4A satellite observations.

However, the reliance of these machine learning methods on mathematical and statistical approaches typically leads to an implicit assimilation of the relationships between cloud properties and radiance observations, making it difficult to trace how input data is transformed into output predictions. A great number of cloud property users favor remote sensing products that offer explicit physical

85 interpretations. Therefore, enhancing traditional inversion algorithms with machine learning algorithms can be beneficial.

In this study, we combine traditional radiative transfer simulations with TIR-CNN retrievals using the OE method (OE-CNN-IR) to retrieve COT, CER, and CTH from MODIS, which is effective under both daytime and nighttime conditions. The Community Radiative Transfer Model (CRTM) is utilized to simulate MODIS IR observations and generate LUT for cloud properties. The TIR-CNN retrievals are employed as a priori states, and an iterative process based on gradient descent is performed to get an optimal estimation. The performance of the proposed OE-CNN-IR model is subsequently compared with a stand-alone OE method utilizing fixed a priori states. Details of the data and the enhanced OE-CNN-IR method are presented in Section 2. Section 3 outlines the retrieval results and their evaluation against cloud products from passive and active sensors. Conclusions are summarized in Section 4.

2 Data and Methodology

2.1 Data

2.1.1 MODIS data

This study utilizes global data observed by MODIS instrument on the Aqua satellite. Aqua-MODIS continuously monitors the Earth-atmosphere system with 36 spectral bands ranging from 0.4 to 14.4 μm. The Aqua-MODIS official Collection 6.1 (C6.1) products (MYD021KM, MYD03, MYD35, MYD06 and MCD12C1), available at https://ladsweb.modaps.eosdis.nasa.gov/search/, have been selected for this study. These products, with spatial resolution of 1 km and 5 km, are chosen for their widely accepted quality (Wang and Christopher, 2003). In this study, the TIR radiation from Aqua-MODIS collection 6.1 (C6.1) Level 1B calibrated radiances products (MYD021KM) are converted to BTs using the Planck function. All channels with wavelength greater than 6.5 μm are used, except that the 30th channel (primarily used for ozone retrievals) is not used to reduce uncertainties induced by ozone. Additionally, atmospheric parameters from MYD03 and MYD06, including surface temperature, land surface type, and cloud phase, are used as ancillary data for LUT construction and forward radiative simulations. The product in Table 1, reported in Cloud Phase Optical Properties is the daytime-only phase used in the MYD06 cloud optical retrievals and Cloud Phase Infrared is a daytime and nighttime product derived from three IR window channel pairs. Cloud Phase Optical Properties is used in daytime to determine cloud types while Cloud Phase Infrared is used in nighttime only in our paper. Cloud optical and physical parameters such as COT, CER and CTH from MYD06 serve to verify the accuracy of daytime retrievals.

All parameters are aligned to a 5-kilometer spatial resolution grid, ensuring uniformity in data and variables. To validate the applicability of the inversion algorithm, retrievals are compared to MYD06 data from one day each month in 2009 (January 1, February 10, March 12, April 11, May 11, June 10, July 10, August 9, September 8, October 8, November 7, and December 7. The default spacing between adjacent days is 30, and the spacing is set to be 40 if a date lies in the same month as previous date), capturing the variability of atmospheric conditions throughout a seasonal cycle and facilitating a comprehensive evaluation across different scenarios. The total sample size of MYD06 for comparison is ~4.7 million. The retrievals are performed over the whole globe, and the data between 60° S-60° N are used in the validation. Table 1 summarizes the data and parameters used in our retrieval model.

Table 1. Summary of MODIS data sources and preprocessing parameters.

Product name	Spatial Resolution	Variables	Unit
MYD021KM	1 km	Band 27 (6.5-6.9 μm)	-
		Band 28 (7.2-7.5 μm)	-
		Band 29 (8.4-8.7 μm)	-
		Band 31 (10.8-11.3 μm)	-
		Band 32 (11.8-12.3 μm)	-
		Band 33 (13.2-13.5 μm)	-
		Band 34 (13.5-13.8 μm)	-
		Band 35 (13.8-14.1 μm)	-
		Band 36 (14.1-14.4 μm)	-
MYD03	1 km	Sensor Zenith	°
		Solar Zenith	°
		Land/Sea Mask	-
MYD06	1 km	Cloud Effective Radius	μm
		Cloud Optical Thickness	-
		Cloud Water Path	$kg\ m^{-2}$
		Cloud Phase Optical Properties	-
		Cloud Phase Infrared	-
	5 km	Cloud Top Pressure	hPa

Surface Temperature		K

2.1.2 Lidar-radar Detection cloud products

Cloud-Aerosol Lidar with Orthogonal Polarization (CALIOP), a space-based lidar instrument onboard the Cloud-Aerosol Lidar and Infrared Pathfinder Satellite Observations (CALIPSO) satellite, provides vertical profiles of clouds and aerosols in Earth's atmosphere. CALIOP can perform observations at both daytime and nighttime, overcoming the limitations of passive optical instruments, but it could not penetrate thick clouds. The Cloud Profiling Radar (CPR) aboard the CloudSat satellite is a radar system that sends out microwave pulses and measures the reflected energy from clouds. This technique is particularly suited to at determining the structure and ice content within clouds, but fails to detect thin clouds. The DARDAR product (Delanoë and Hogan, 2010), integrating data from both CALIOP and CPR, offers a comprehensive atmospheric column view that neither instrument can achieve independently. This extensive dataset includes information on cloud top and base heights, optical thickness, ice content, and aerosol layers. In our study, the ice cloud product of DARDAR in 2009 is used to evaluate the inversion results during both daytime and nighttime conditions, and ~0.54 million pixels are collocated in the comparison processes.

2.2 Development of the retrieval algorithm

The core algorithm of our inversion method is the optimal estimation method, which utilizes the CRTM as the forward model and incorporates CNN results as a prior information. Figure 1 illustrates the architecture of our retrieval models. Initially, temperature, humidity and ozone from the Fifth Generation of the European Centre for Medium-Range Weather Forecasts (ECMWF) Reanalysis (ERA5) (Hersbach et al., 2020) are used to construct lookup tables for each 0.25°×0.25° spatial grid box. These LUTs enumerate the BT for each channel corresponding to varying COT, CTH and CER. Subsequently, the OE method is performed to retrieve cloud properties. The OE method can get the optimal solution by accounting for all spectral information. However, the iteration may have started a long way from the solution in nonlinear problem and the cost function decrease is much slower. Start with a better first guess rather than climatology value can make the process converges much more quickly (Rodgers, 2000). The deep learning methods can achieve high accuracy, and once trained, they offer very fast prediction speeds. However, due to the nature of neural networks, deep learning results often lack interpretability, leading

to the perception of deep learning as a black box model. In OE-CNN-IR approach, the TIR-CNN derived cloud properties provide a priori states for iterative processes, which is subsequently refined through iterative minimization of the objective cost function, while the climatology values were used as starting

155 points in OE-IR. This method iteratively adjusts parameters to reconcile radiative transfer simulations with observed data. Further details are presented below.
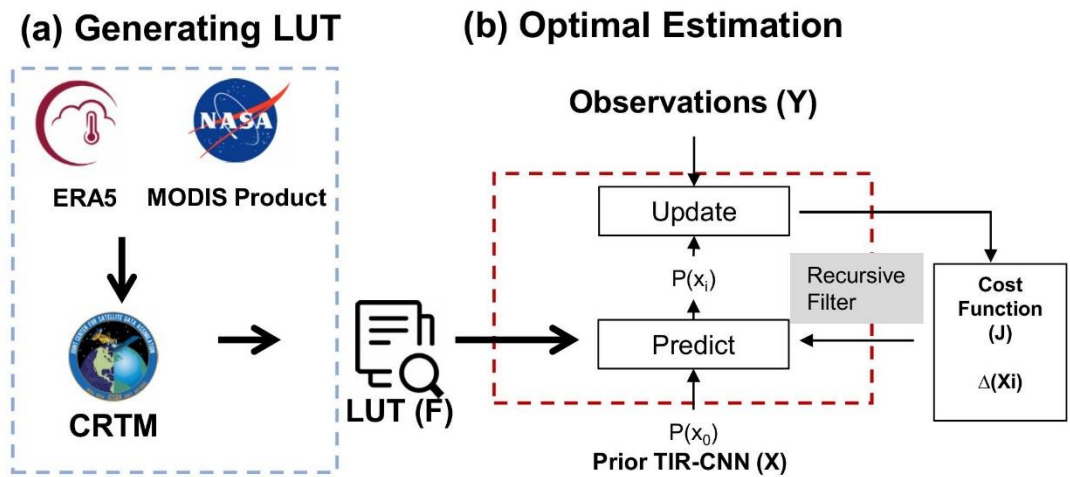
Figure 1. The architecture of the retrieval model. (a) The establishment of look-up table. (b) The iteration steps in the optimal estimation progress.

160 **2.2.1 Forward Model**

The CRTM, developed by the U.S. Joint Center for Satellite Data Assimilation (JCSDA), spans a broad spectrum of channels from visible to microwave. It is widely used in simulating radiances at the top of the atmosphere for various satellite sensors, owing to its flexible interface, sophisticated radiative transfer processes, and efficient numerical computation (Han et al., 2006). The model divides the atmosphere into

165 a series of vertical layers, and the temperature, pressure and composition of each layer is assumed to be homogenous. CRTM solves the radiative transfer equations throughout the atmosphere. Its precision and reliability have been extensively validated by ground-based and satellite observations (Zou et al., 2016). Considering that the optical properties of ice cloud crystals in the CRTM and MODIS products differ due to variations in particle habit assumptions (Yi et al., 2016; Yao et al., 2018), the volumetric extinction

170 cross section in the CRTM is adjusted by a scaling factor of 0.4, resulting in simulated brightness temperatures that are consistent with observations (Fig. 6(a, b, c)). For each grid cell, the CRTM simulates TIR radiances corresponding to a set of COT, CER, and CTH values at each location, from

which a LUT is subsequently constructed. Table 2 provides a detailed list of the cloud properties and ancillary parameters used in these calculations.

175 **Table 2. Geometries and cloud properties selected to calculate the cloud lookup tables**

	Variable Names	Notes
Reference cloud properties	COT	0.01, 0.03, 0.05, 0.10, 0.20, 0.30, 0.40, 0.50, 0.60, 0.70, 0.80, 0.90, 1.00, 1.20, 1.40, 1.60, 1.80, 2.00, 2.50, 3.00, 3.50, 4.00, 4.50, 5.00, 5.50, 6.00, 6.50, 7.00, 7.50, 8.00, 8.50, 9.00, 9.50, 10.0, 12.0, 15.0, 20.0, 25.0, 30.0, 50.0
	CER (μm)	5, 10, 15, 20, 25, 30, 35, 40, 45, 50, 55, 60, 65, 70, 75, 80, 85, 90
	CTH (km)	0.1, 0.8, 1.15, 1.5, 2, 2.5, 3.5, 5, 6.25, 8, 10, 12, 14, 16
Model parameters	Surface temperature (K)	MYD06
	Land type	MCD12C1, IGBP
	Cloud type	MYD06, Cloud Phase
	Temperature profile (K)	ERA5, Temperature
	Water vapor profile (g kg^{-1})	ERA5, Specific humidity
	Ozone profile (g kg^{-1})	ERA5, Ozone mass mixing ratio

The outputs of the forward model (F) can be expressed as a function of cloud properties and ancillary parameters:

$$Y = [BT_1 BT, BT_2, \dots \dots, BT_m]^T = F[X(COT, CER, CTH), P] + e, \tag{1}$$

180 where Y is a vector consisting of m MODIS IR observations of BT, P is a vector encompassing various ancillary variables, including air temperature, water vapor concentration, ozone concentration profiles, surface emissivity spectrum, and surface temperature. The state vector (X) includes COT, CER and CTH, and e is an error term.

Figure 2 depicts the variation in CRTM output (F) (expressed in BT) as a function of ice cloud properties, derived from a simulation using the atmospheric profile dated June 10, 2009, at 00:00 UTC, at coordinates 175.87° E and 60.55° N. In Fig. 2(a), with fixed CER and CTH, the TOA BTs in MODIS IR bands generally decrease with increasing COT. Notably, for COT>10, the slopes approach zero, causing challenges in inversion accuracy. In the case of fixed COT and CTH (Fig. 2(b)), TOA BTs decrease with increasing CER values when CER is below 10 μm across all channels, followed by minor oscillations in most channels, except that band 29 shows significant variations. In Fig. 2(c), for CTH values under 11 km, TOA BTs are negatively correlated with CTH noticeably.

Figure 3 shows the relationship between TOA BTs and liquid cloud properties, which reveals a weaker response to changes in COT and CER compared to ice clouds. Nevertheless, TOA BTs decrease noticeably with increasing liquid cloud CTH. In summary, CTH is the most accurately determinable variable for both ice and liquid clouds due to the high sensitivity of TOA BTs to CTH. For ice clouds, COT values below 10 generally allow for more accurate retrieval of cloud properties in theory. However, retrieving CER for ice clouds poses greater challenges due to the complexity of ice particle size distribution and shape. Liquid clouds, conversely, show no strong sensitivity of TOA BTs to both COT and CER, and it is more difficult to accurately retrieve these cloud properties solely based on TOA BT observations.
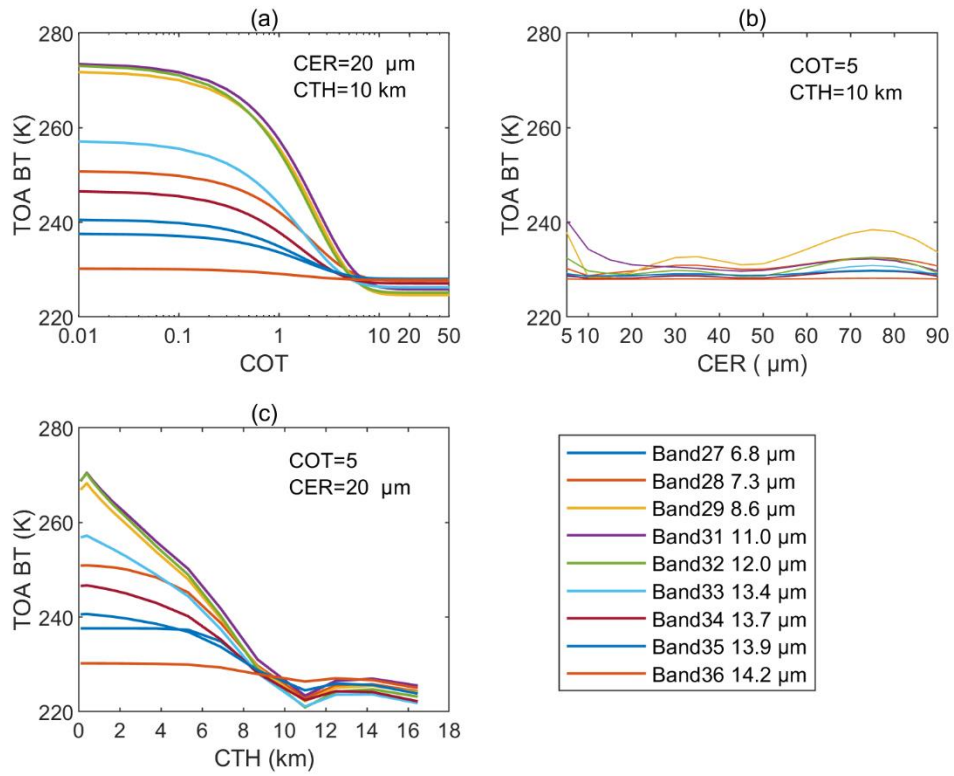
Figure 2. Radiative transfer model simulations for ice clouds. The atmospheric profile is from the coordinates with a longitude of 175.87° E and a latitude of 60.55° N, on June 10, 2009, at 00:00 UTC. (a) TOA BTs as a function of COT, when CER and CTH is set to 20 μm and 10 km, respectively. (b) BT as a function of CER, when COT and CTH is set to 5 and 10 km, respectively. (c) BT as a function of CTH, when COT and CER is set to 5 and 20 μm, respectively.
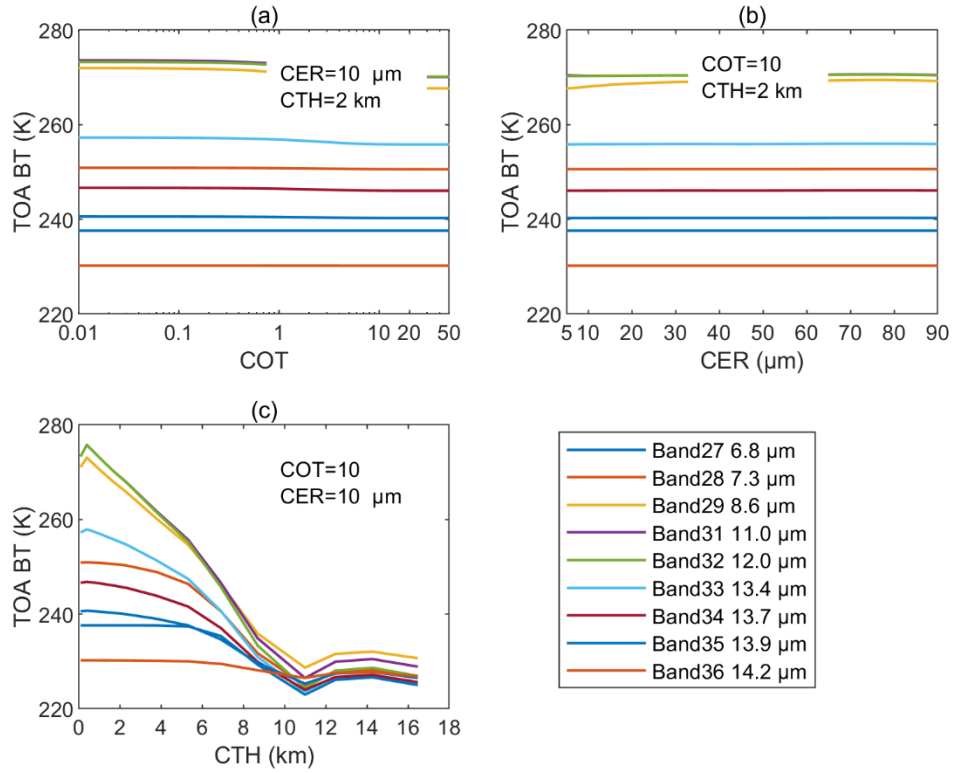
Figure 3. Same as Fig. 2, but for liquid clouds.

2.2.2 The Convolutional Neural Network Infrared method

210 The convolutional neural network using thermal infrared (TIR-CNN) model is trained with solar-independent variables (thermal infrared radiances, viewing zenith angles, and altitude) as inputs and uses standard MYD06 products (COT, CER and CTH in the daytime) as targets. To capture a comprehensive range of the Earth's surface and viewing geometries while accounting for seasonal variations, Wang et al. (2022) collected full-year granules from 2010 to create the training dataset. Products with a 10-day

215 interval from 2011 were selected as the validation dataset during the training phase. Additionally, the 10-day interval data from 2009, which is independent of both the training and validation datasets, served as the testing dataset. The granules were divided into samples sized 256 × 256 km. After preprocessing, there are 1,888,680 samples in the training dataset, 191,520 in the validation dataset, and 382,760 in the testing dataset. This TIR-CNN model is an asymmetric architecture, featuring an equal number of

220 encoding and decoding layers arranged sequentially. The basic convolutional block consists of two 2D convolutional layers with 3 × 3 kernels. Each convolutional layer is followed by a batch normalization layer and a leaky rectified linear unit (Wang et.al.,2022). Through training, the model can capture context

and learn the complex nonlinear relationship between the input variables and targets, which can be applied in the cloud property retrievals during both daytime and nighttime. The convolutions in the TIR-CNN model are beneficial in considering statistic information from neighbor fields in training. Theoretically, spatial distributions, optical and microphysical properties of clouds are all determined by the meteorological backgrounds, so cloud properties are statistically connected to their horizontal distributions. In addition, the effective radius of ice cloud particles are functions of cloud temperature. The CNN-based deep learning architecture is able to capture the statistical features among adjacent pixels of satellite observations as a solution for retrieving cloud optical and micro-physical properties (Wang et al., 2022, 2023), so it is able to provide more information than traditional algorithms that retrieve cloud properties from infrared radiances of individual pixels. The benefits of machine learning in IR cloud retrievals have also been demonstrated independently by the results of Tana et al. (2023) and Zhao et al. (2023).

2.2.3 Optimal Estimation-Based Retrieval Method

The OE-based retrieval method, as introduced by (Rodgers, 2000), is designed to derive the best estimates of atmospheric quantities (such as temperature, humidity, aerosol concentration, or trace gas concentrations) by minimizing the discrepancy between observed measurements and the model simulations. This method combines information from both the measurement data and a priori knowledge, typically obtained from atmospheric models or ancillary data sources. A key strength of the OE method is its capability in addressing complex atmospheric retrieval challenges, enabling simultaneous retrieval of multiple parameters in contexts where physical processes are nonlinear and highly coupled. It provides a rigorous and statistically robust method to estimate atmospheric parameters, along with quantifying the associated uncertainties.

The OE method aims to identify the most probable state variables by minimizing a cost function J (Wang et al., 2016a):

$$J = [F(X,P) - Y]^T S_y^{-1} [F(X,P) - Y] + [X - X_a]^T S_a^{-1} [X - X_a], \tag{2}$$

where X_a and X are the prior and posterior state vectors, respectively. S_y and S_a are the covariance matrices of the observation-to-simulation differences and the uncertainty of the prior state vector, respectively. When the uncertainties of a priori state are large (e. g., OE-IR), the cost function J is

primarily influenced by the first term in OE-IR. If the uncertainties of a priori state are small, then the second term is also important in the iteration process (e. g., OE-CNN-IR). Then we employ an iterative process to find an optimal solution based on observed data and a priori states. In this paper, the gradient descent method for *(i+1)*'th iteration is implemented by:

$$X_{i+1} = X_i - \theta \frac{\partial J_{i,n}}{\partial x_{i,n}} \ , \tag{3}$$

where

$$\frac{\partial J_{i,n}}{\partial x_{i,n}} = \frac{J(X_{i,n} + \delta x_n) - J(X_{i,n})}{\delta x_n} \ , \tag{4}$$

and θ represents a learning rate and n represents the n-th cloud parameters (COT, CER and CTH), and θ is set to be the same for all three variables. In this paper, θ is initially set to 0.05 for the first 200 iterations and after those initial 200 iterations, the learning rate is then reduced to 0.01 for the subsequent 100 iterations. δx_n represent the small increase in n cloud parameters and $J(X_{i,n} + \delta x_n)$ are calculated using LUTs.

In this paper, stand-alone OE-IR method relies on a fixed a priori value for its iterative process, whereas OE-CNN-IR utilizes results from TIR-CNN as it's a priori states for further refinement. These methods illustrate the integration of traditional optical estimation techniques with advanced machine learning models to potentially enhance the accuracy and reliability of atmospheric measurements.

Figure 4 shows the iterative variations in cost function, COT, CER and CTH for both OE-IR and OE-CNN-IR under various conditions. Both algorithms show a significant decrease with an increasing number of iterations and all iterations can achieve successful convergence. However, the initial value for OE-CNN-IR is lower than OE-IR. For smaller cot values (COT < 10), OE-CNN-IR and OE-IR exhibit consistent effects on COT and CTH, converging with close values. For both methods, the CER depends on a priori states. A distinct difference is that OE-CNN-IR starts with a significantly lower cost than OE-IR and maintains more stability throughout the iteration process. For larger COT values (COT > 10), the CTH of these two methods converge to same value, despite of differences in a priori states. The COT of OE-IR struggles to iterate towards the expected target during the iteration process, while OE-CNN-IR maintains stably around the a priori values. The iterative results indicate that both methods perform well on COT and CTH for small COT values. However, for large COT values, the OE-IR method is unable to produce accurate results under these conditions. In contrast, the OE-CNN-IR is able to retrieve COT of thick clouds effectively.
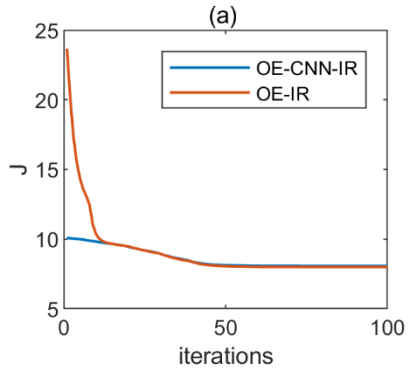
A thin cloud case   **A thick cloud case**
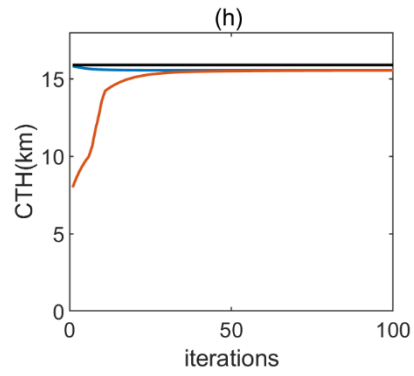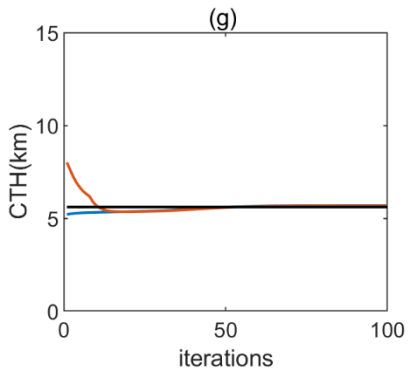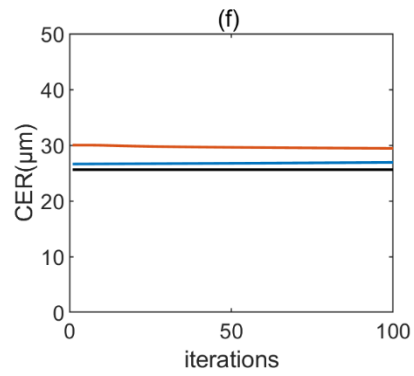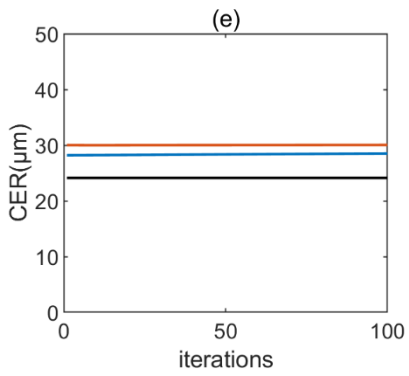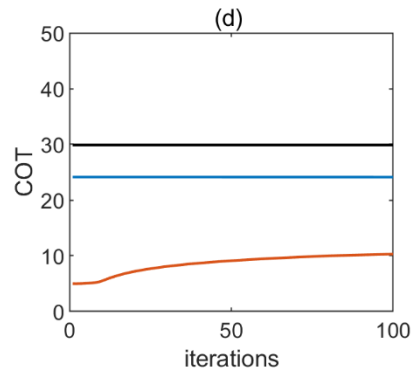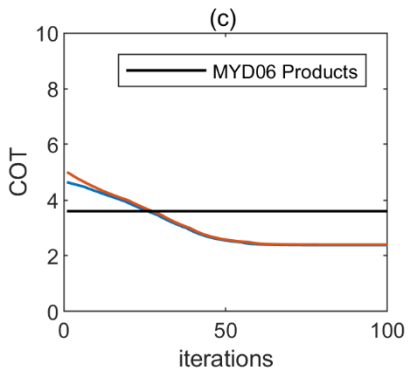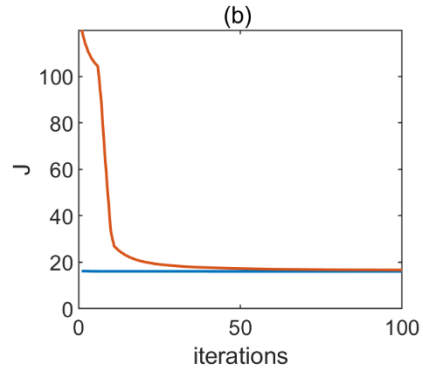
Figure 4. The change of cost function and cloud parameters in the iteration processes, with OE-IR in Red and OE-CNN-IR in Blue. Left pictures are for an illustrative ice cloud layer with a small optical thickness case and right pictures are for a large optical thickness case.

285 **2.3 Metrics for performance evaluation**

In this study, the magnitude of calculation errors, systematic bias errors, and linear correlation between outputs and standard values are quantitatively assessed using three key statistical metrics: root mean squared error (RMSE), mean bias error (MBE), and the Pearson correlation coefficient (r).

$$RMSE = \sqrt{\frac{\sum_{i=1}^{N}(y_i - f_i)^2}{N}} \ , \qquad (5)$$

290 $$MBE = \frac{\sum_{i=1}^{N} f_i - y_i}{N} \ , \qquad (6)$$

$$r = \frac{\sum_{i=1}^{N}(f_i - \bar{f})(y_i - \bar{y})}{\sqrt{(\sum_{i=1}^{N}(f_i - \bar{f})^2)}\sqrt{(\sum_{i=1}^{N}(y_i - \bar{y})^2)}} \ , \qquad (7)$$

where N is the total number of calculated points, y and f are the true and estimated values, respectively.

3 Results and discussion

295 **3.1 Case studies of OE-CNN-IR and OE-IR retrievals**

To illustrate the daytime efficacy of the proposed method, a granule from Aqua-MODIS, captured at 03:00 UTC on June 10, 2009, has been chosen. This particular granule spans the southwestern Pacific Ocean, encompassing the geographical region from 0° to 20° S latitude and from 150° E to 175° E longitude, as depicted in Fig. 5.

300   Figures 5 (a-c) show the spatial distribution of BT for each respective channel. These measurements reveal variations in thermal radiation, which correlated with cloud properties specific to the wavelengths of the channels used. Figures 5(d-f) show the cloud physical properties as derived using standard MODIS retrieval algorithms. The COT, CER, and CTH from the MYD06 product provide a benchmark for comparison with other inversion methods. The analysis of BT from channels 29, 31, and 32 shows a clear

305 negative correlation with both COT and CTH, and regions with higher BT typically correspond to clouds with smaller optical thickness and lower cloud top heights. This is in line with the principle that thinner clouds permit more infrared radiation to escape from the Earth's surface and atmosphere, leading to higher observed BT. Furthermore, the analysis indicates that clouds with higher BT generally have lower

altitudes. The patterns in Fig. 5, which display cloud properties derived from various inversion techniques,

310   corroborate the physical relationships illustrated in Figs. 2 and 3. Figures 5 (g-i) present the retrieval

results from the deep learning algorithm TIR-CNN method. The CNN-derived retrievals are not only

consistent with MYD06 products in spatial patterns, but also agree well with the magnitudes of results.

Figures 5 (j-l) present the retrieval results from the OE-CNN-IR method, showing similar spatial

distributions to the standard MYD06 products for COT and CTH. However, significant differences are

315   noted in CER retrieved by OE-CNN-IR and MYD06 products. This finding aligns with the work of Wang

et al. (2016), which highlighted substantial discrepancies in CER retrieval when using OE-IR versus

VNIR/SWIR/MWIR methods. Specifically, the C6 MYD06 cloud particle size information presented

here is inferred from the 2.1 μm reflectance, which may capture signals reflected from the lower parts of

a cloud (Zhang et al., 2009).

320   Figures 5 (m-o) show the results retrieved using the traditional OE-IR method with climatological

priori states, which employs climatological values of COT, CER and CTH as a priori states for OE

iteration. In case where COT values are below 10, the OE-IR COT closely match MYD06 products,

indicating that it is able to capture the COT of thinner clouds. However, the inability of OE-IR to retrieve

COT values greater than 10 suggests a limitation in the technique's sensitivity to optically thicker clouds,

325   aligning with findings from Wang et al. (2016). This threshold effect arises from the TIR BT

independence to COT in thick clouds (as shown in Fig. 2a). The performance of CTH retrievals using

the OE-IR method is comparable to that of the OE-CNN-IR method while the inversion of CER is not

very effective due to limitations in the physical mechanisms.
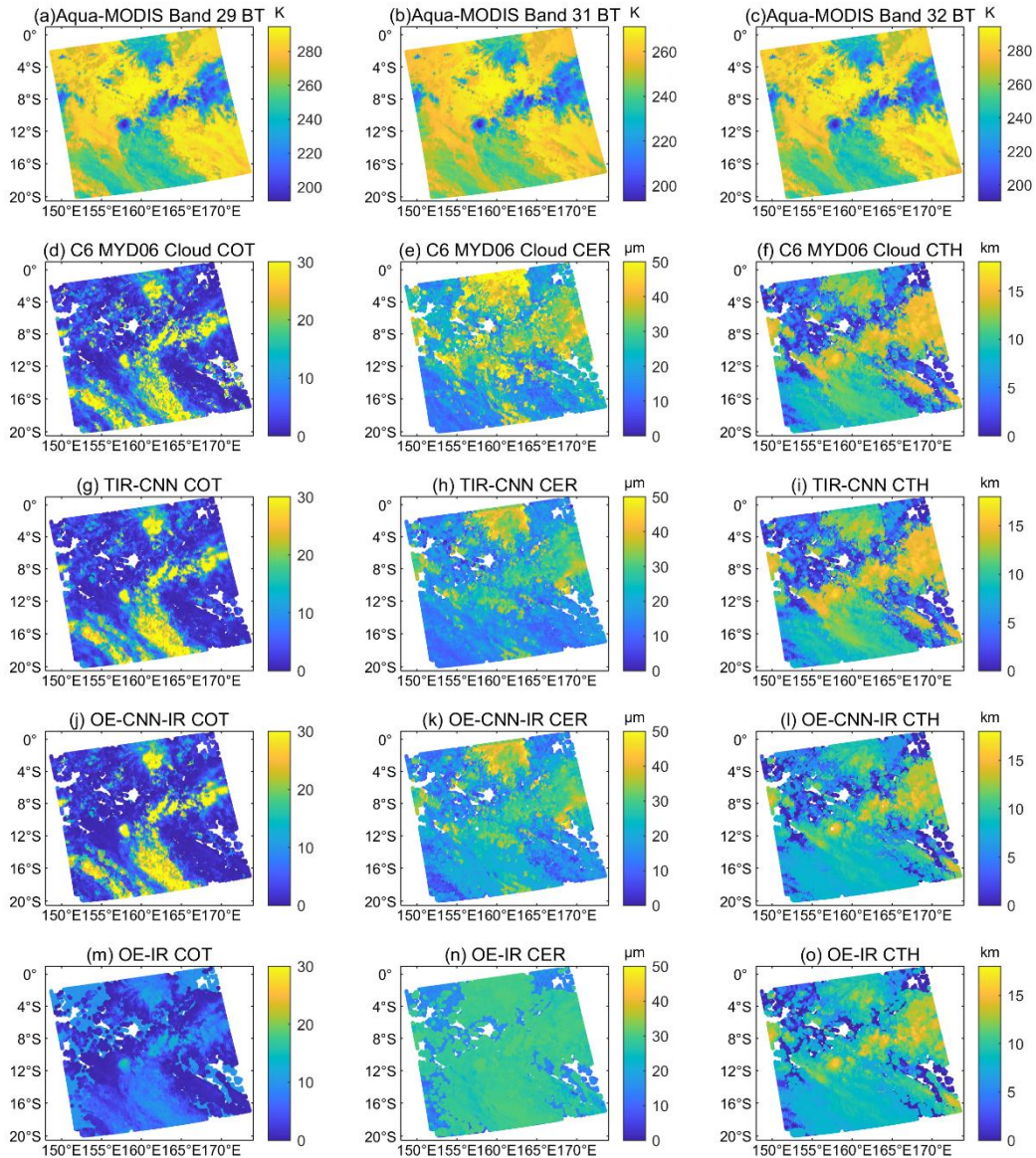
330

Figure 5. Comparison of cloud properties obtained from the TIR-CNN model, OE-CNN-IR model, OE-IR model and standard MODIS products for an illustrative daytime granule on 10 June. 2009 (03:00 UTC). (a, b, c) are BT image of MODIS band 29, 31 and 32, respectively. (d, e, f) are the COT, CER, and CTH from the MYD06 product, respectively. (g, h, i) are the COT, CER, and CTH from the TIR-CNN model, respectively.

335 **(j, k, l) are the COT, CER, and CTH from the OE-CNN-IR model, respectively. (m, n, o) are the COT, CER, and CTH from the OE-IR model, respectively.**

Figure 6 compares MODIS observed BTs with simulated BTs derived from CRTM. Figures 6(a-c) show CRTM-simulated radiances using baseline MODIS cloud products, serving as a control scenario for comparative analysis. The correlation coefficients for channels 29, 31, and 32 are 0.877,0.905 and 0.891,

340 respectively, indicating CRTM's proficiency in simulating MODIS cloud products. However, there is a

persistent negative MBE across these channels. Figures 6(d-f) present a comparison between observations and BT simulated by CRTM and TIR-CNN retrievals, with outcomes that are analogous to those depicted in Figs. 6(a-c). The pronounced correlation indicates that CNN-based inputs proficiently replicate the spatial and radiometric features of clouds, showing high consistency with MODIS MYD06

345 products. When OE-CNN-IR or OE-IR cloud property retrievals are used to simulate BT, the correlation coefficients between the simulated BT and observations increases significantly, and the absolute values of MBE and RMSE decreases significantly (as shown in Figs. 6g-l). The OE-CNN-IR model incorporates the OE iterations, which reduce the discrepancy between simulated and observed BT. The results indicate that retrievals of the OE-CNN-IR methods align more closely with BT observations compared to the

350 stand-alone TIR-CNN model.
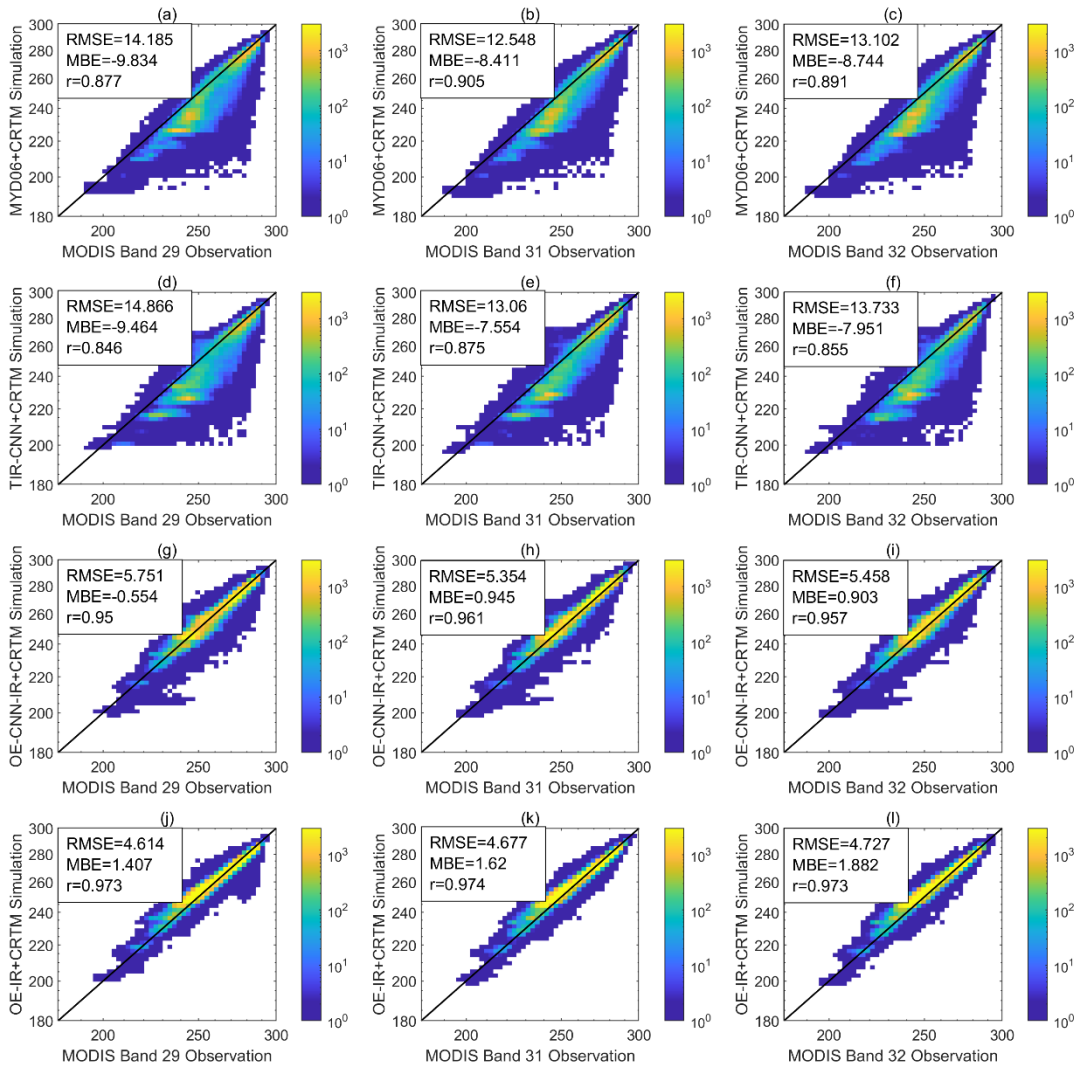
355

Figure 7 illustrates a nighttime case of cloud parameter retrievals using TIR-CNN, OE-CNN-IR and

360 OE-IR methods. The data for this analysis is sourced from a randomly selected granule captured on

February 10th, 2009, at 21:00 UTC. Figures 7(a-c) display the BTs at channels 29, 31, and 32, and Figs.

7(d-f) show the COT, CER, and CTH retrieved by the TIR-CNN algorithm. The relationship between

COT and CTH with BT at night is generally consistent with that during the day. Figure 7(g-i) shows the

COT, CER, and CTH retrieved by the OE-CNN-IR algorithm. The OE-CNN-IR retrievals align well with

365 the high and low-value areas in the BT images, indicating that OE-CNN-IR effectively discerns the

intricate spatial variations in cloud properties during nighttime conditions. Figures 7(j-l) display the cloud

parameters retrieved using the OE-IR method. In this analysis, the predominance of values falls below

10, which signifies a more constrained retrieval scope when contrasted with the OE-CNN-IR method.

Nevertheless, the distribution of CTH derived from OE-IR closely mirrors that obtained from OE-CNN-

370 IR, affirming its dependability for estimating the top height of clouds. Additionally, both methods exhibit

comparable distributions in CER.
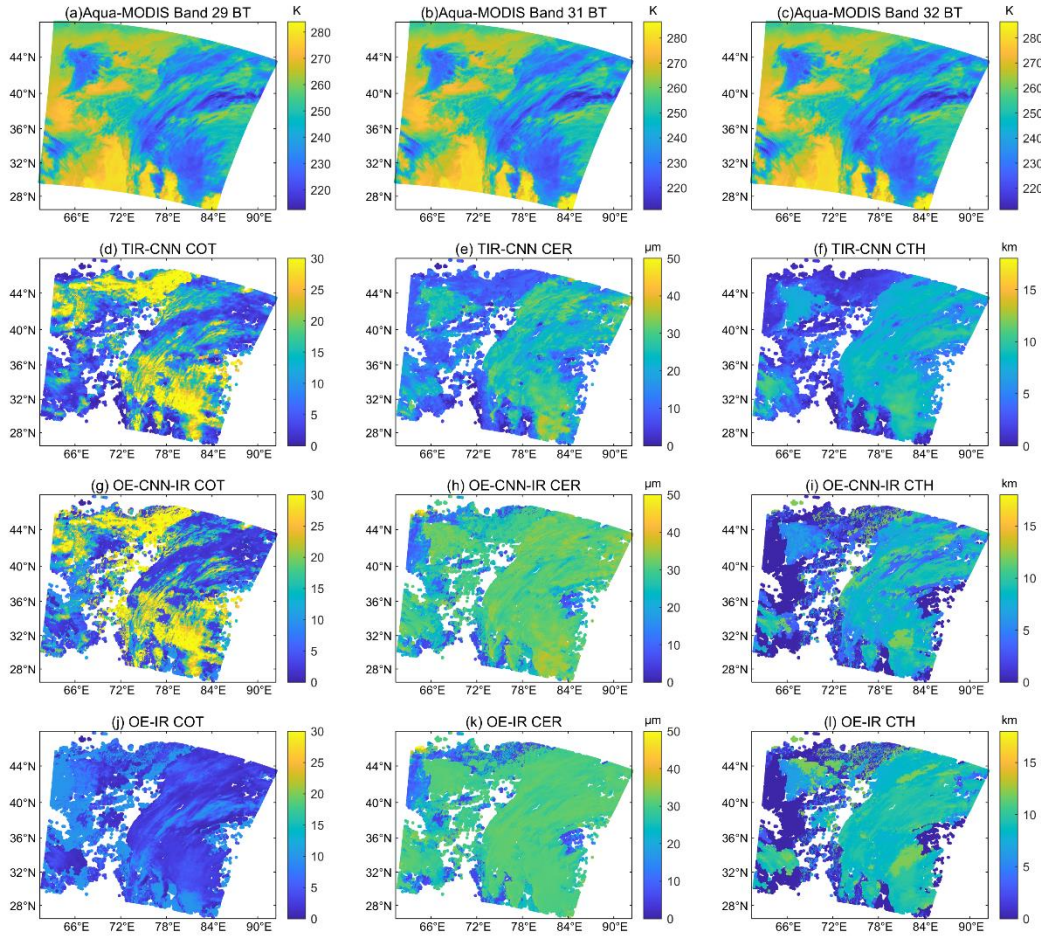
Figure 7. Comparison of cloud properties obtained from the OE model and standard MODIS products for an illustrative nighttime granule on 10 February 2009 (21:00 UTC). (a) BT image of MODIS band 29. (b) BT image of MODIS band 31. (c) BT image of MODIS band 32. (d, e, f) are the COT, CER, and CTH from the TIR-CNN, respectively. (g, h, i) are the COT, CER, and CTH from the OE-CNN-IR model, respectively. (j, k, l) are the COT, CER, and CTH from the OE-IR model, respectively.

3.2 Comparison between retrievals and MYD06 products in the daytime

Figure 8 presents scatterplots that provides pixel-level comparisons of cloud property retrievals from OE-CNN-IR and OE-IR against the MYD06 ice cloud products over ocean for 2009. The left column of Fig. 8 offers a detailed pixel-by-pixel comparison for COT, CER, and CTH between OE-CNN-IR and the MYD06 ice cloud products. The middle column displays comparisons between MYD06 cloud products and OE-IR retrievals. The right column displays the probability density functions obtained from MYD06 products, OE-CNN-IR and OE-IR derived results. The color scale in these plots indicates the number of observations in each grid, visually representing data point density. Due to the large uncertainties of MODIS in retrieving COT in polar regions, retrieval constraints have been established.

These include limiting the Solar Zenith Angle (SZA) to less than 60 degrees and restricting latitudes to between 60° S and 60° N, thereby ensuring consistency and reliability in these comparisons. In Fig.8(a), the correlation coefficient between OE-CNN-IR COT and MYD06 COT is 0.835, indicating a strong positive correlation. In comparison, OE-IR achieves a COT correlation coefficient of 0.667 against MODIS products, indicating a slightly weaker relationship than that reported in Wang et al. (2016). In Fig.8(c), the distributions provided by MYD06, OE-CNN-IR, and OE-IR are relatively similar for COT values less than 10. The OE-CNN-IR retrievals contains a lot of cases with COT>15, which is consistent with MODIS, but OE-IR retrievals do not contain clouds with COT>15. The underestimation of COT for thick clouds by OE-IR is consistent to Wang et al. 2016. Therefore, it is concluded that both OE-CNN-IR and OE-IR show consistent performance for COT below 10, but OE-CNN-IR performs much better for thicker clouds. With respect to CER, both algorithms demonstrate moderate to weak correlation coefficients, reflecting the inherent physical constraints of the retrieval process. Nonetheless, OE-CNN-IR outperforms OE-IR with a correlation coefficient of 0.794, suggesting enhanced performance. In Fig.8(f), the results from OE-IR appear to be concentrated around a priori value of 30 μm, whereas the results from OE-CNN-IR maintain a distribution that is more similar to that of MYD06. For CTH retrieval, both OE-CNN-IR and OE-IR demonstrate good performance, with correlation coefficients of 0.871 and 0.808, respectively. Overall, the statistical analysis in Fig. 8 underscores the retrieval capability of OE-CNN-IR, particularly for COT and CER, compared to stand-alone OE-IR.

Figure 9 expands the ice cloud analysis from Fig. 8 to encompass liquid and ice clouds over both land and ocean, offering a more comprehensive evaluation of the retrieval algorithms across varied cloud conditions. In the case of liquid clouds above 10, the BT is not sensitive to COT, leading to most OE-IR COT retrievals clustering around value of 10. This indicates difficulties in effectively retrieving COT for liquid clouds, so the OE-IR method has been used to retrieve cloud properties of ice clouds only. In contrast, the performance of OE-CNN-IR is much better. This shows OE-CNN-IR can be improved by using TIR-CNN outputs as a priori state, allowing for accurate retrievals even in situation of lower BT sensitivity, as observed in liquid clouds. Regarding CER, the gradient of CER with respect to BT of liquid clouds tends toward zero. These artifacts signal the limitations of the retrieval algorithm under minimal BT gradient conditions. Despite these challenges for CER, both OE-CNN-IR and OE-IR perform

415   exceptionally well in retrieving CTH, with correlation coefficient of 0.913 and 0.931, respectively. These

high correlations reflect the algorithms' effectiveness in estimating CTH.
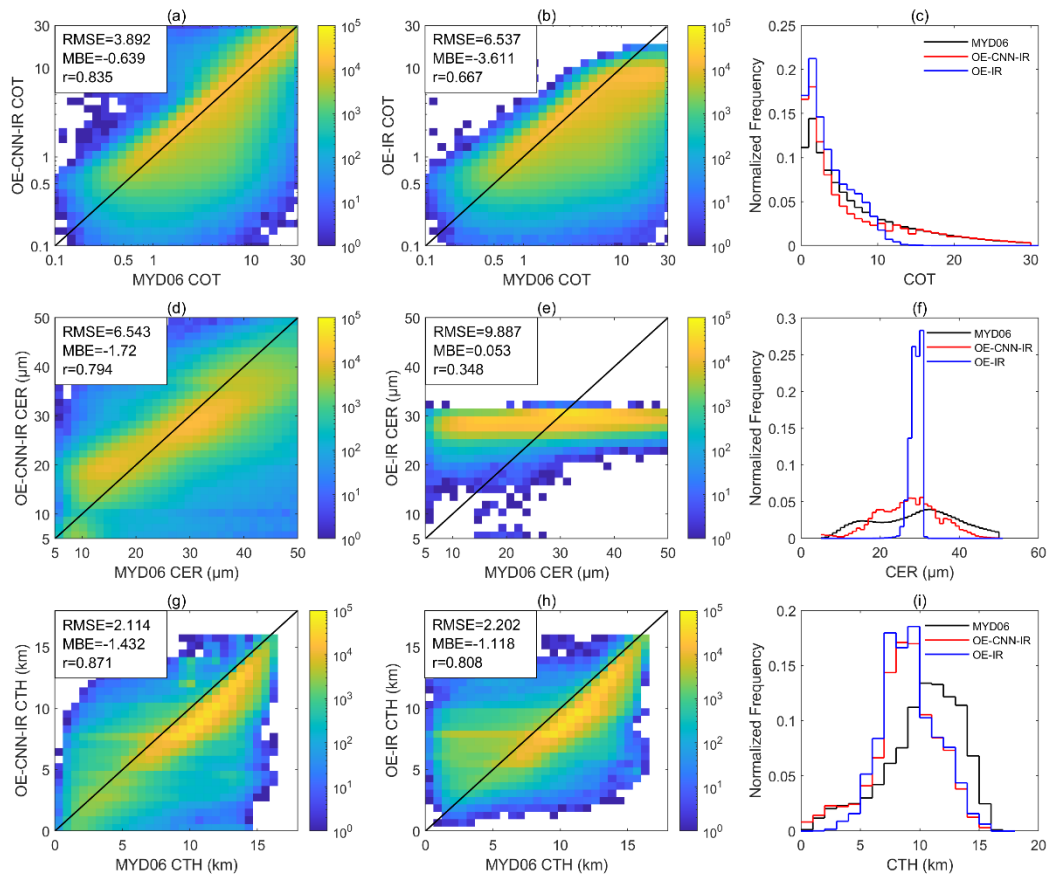
Figure 8. Scatterplots of the pixel level comparisons between the retrievals and MYD06 products for ice clouds over oceans. (left column) Pixel-by-pixel comparisons of COT, CER, and CTH from OE-CNN-IR with the MYD06 ice cloud products over ocean in 2009. (middle column) Scatterplots of the pixel level comparisons between the MYD06 cloud products and OE-IR comparable retrievals. (right column) The probability density functions obtained from MYD06 products, OE-CNN-IR and OE-IR derived results are presented. Color shadings denote the number of observations in each respective pixel. All comparable retrievals are constrained to cases with SZA < 60° and latitude between 60° S and 60° N.
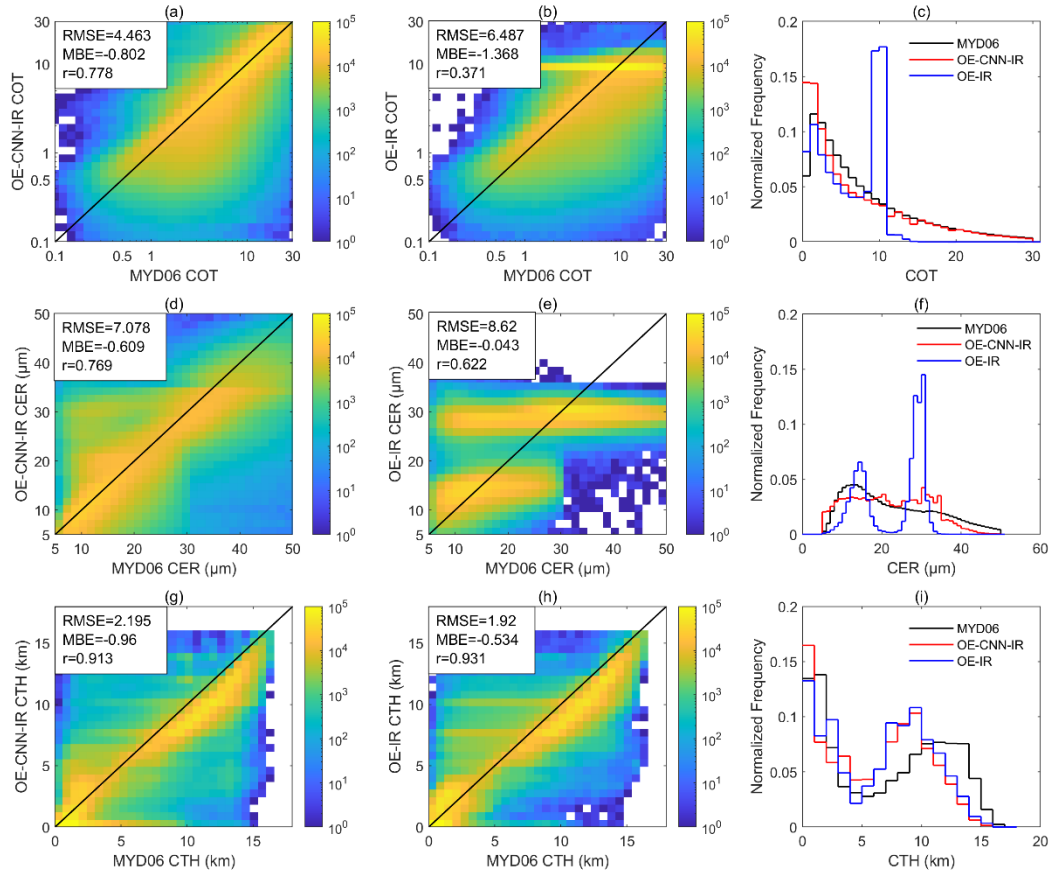
Figure 9. Same as Fig. 8, but includes liquid clouds over ocean, and ice and liquid clouds over land.

3.3 Comparison with products from active sensors

Under nighttime conditions, where standard MYD06 cloud products do not offer cloud optical properties, the evaluation is supplemented by incorporating near-real-time data from active sensors (DARDAR, derived from CloudSat/CALIPSO observations). Spatially and temporally co-located samples from 2009 are employed to evaluate the performance and generalization capabilities of the OE model during night conditions. These criteria are applied to achieve the closest possible data correspondence between the two different instruments, facilitating a meaningful assessment of the OE model's nighttime performance.

Figure 10 presents a detailed comparison of COT retrievals for ice clouds using OE-CNN-IR and OE-IR methods, benchmarked against DARDAR cloud products. The comparisons are confined to latitudes between 60° N and 60° S to ensure a comprehensive assessment across both daytime and nighttime conditions. The daytime correlation coefficient for OE-CNN-IR versus DARDAR COT is 0.651, with slightly lower nighttime correlation of 0.583. These values are similar to the correlation between MYD06 COT and DARDAR COT (0.647). In contrast, OE-IR exhibits lower correlation

440   coefficients, with 0.546 during the day and 0.503 at night. Nevertheless, the RMSE of OE-IR is lower

than that of OE-CNN-IR. Notably, the OE-CNN-IR method demonstrate better performance for COT >

10. This suggests that OE-CNN-IR is more adept at capturing the variability of thicker ice clouds, which

is important for understanding cloud radiative effects and their implications for weather and climate

systems.
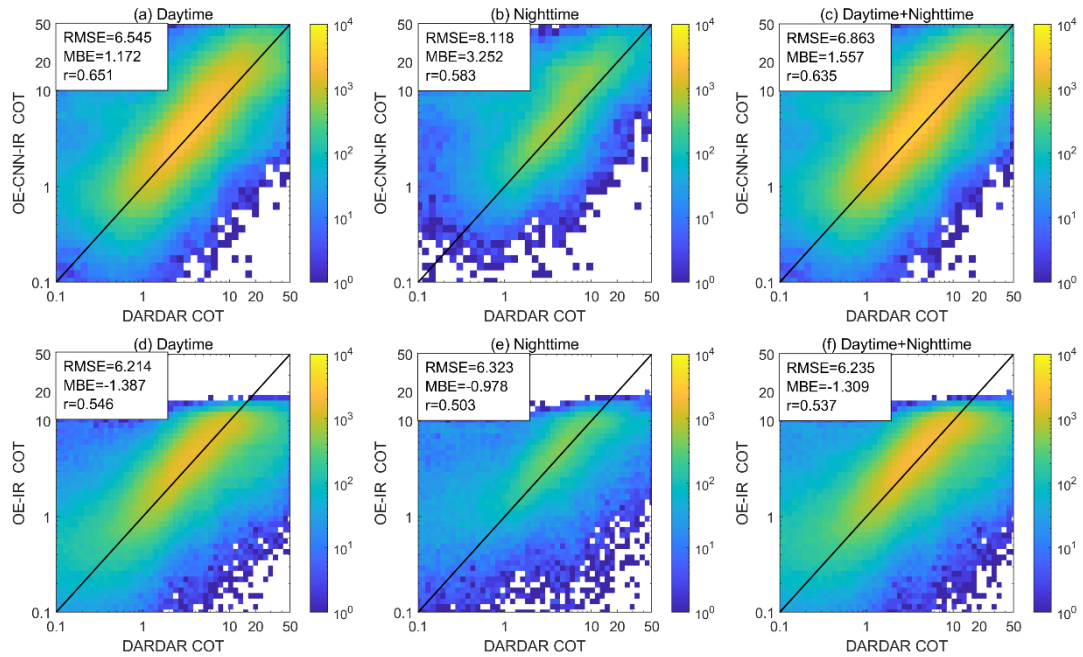
445

Figure 10. Comparisons of OE-CNN-IR COT, OE-IR COT and DARDAR COT for ice clouds over oceans. (a-c) are comparisons between OE-CNN-IR COT and DARDAR products. (d-f) are comparisons between OE-IR COT and DARDAR products. The left column is for daytime comparisons, the middle column is for nighttime comparisons, and the right column is for all-day comparisons.

450   **4   Conclusions**

This study introduces a cloud property retrieval method based on optimal estimation (OE-CNN-IR), which integrates traditional radiative transfer simulations with a machine-learning method. Designed for retrieving COT, CER, and CTH, this method is applicable for passive satellite imagery under both daytime and nighttime conditions. Retrievals from a machine learning algorithm (TIR-CNN) are used to

455   provide a priori values for OE iteration, and an RTM is used to create radiance lookup tables that are used in the iteration processes. Subsequently, the retrievals are iteratively adjusted to minimize discrepancies between the IR observations and radiative transfer model simulations. The efficacy of OE-CNN-IR is validated against MYD06 products and active sensor cloud products, and the results are compared to a stand-alone optimal estimation model (OE-IR).

460   The validation results reveal that the OE-CNN-IR method outperforms stand-alone OE-IR model, especially for cloud optical thickness of thick clouds, due to it's better a priori values. Correlation coefficients with MYD06 products have exhibit marked improvements: correlation coefficients for COT increases from 0.667 to 0.835, correlation coefficients for CER increases from 0.348 to 0.794, and correlation coefficients for CTH increases from 0.808 to 0.871. In nighttime evaluations, the OE-CNN-

465   IR method consistently outperforms the traditional OE model when compared with DARDAR COT. The consistency between OE-CNN-IR retrievals and MYD06 products is as good as that of stand-alone machine-learning retrieval algorithm (i. e., TIR-CNN), and the radiance simulations based on OE-CNN-IR retrievals exhibit greater consistency with actual observations, as depicted in Fig. 6. Furthermore, the algorithm explicitly addresses physical processes, aligning with the preferences of scientists who

470   advocate for physically based methodologies. While the OE-CNN-IR method in this study is primarily applied to Aqua-MODIS imagery, it can be potentially applied to other sensors with similar infrared (IR) channels. For instance, it can be readily adapted to geostationary satellites, given their analogous wavelength ranges (Tana et al., 2023; Zhao et al. 2023). In the future, the combination of machine-learning algorithms and traditional radiative transfer simulations might be further developed in other

475   fields of remote sensing.

Code/Data availability

The custom code/data used in this study is available upon reasonable request from the corresponding author and related OE codes are available at https://github.com/huanghe141327/Codes-for-Huang-et-al..

Competing interests

480   The authors declare that they have no conflict of interest.

Credit authorship contribution statement

He Huang: Methodology, Data curation, Validation, Formal analysis. **Quan Wang:** Data curation, Writing – review & editing. **Chao Liu:** Writing – review & editing. **Chen Zhou:** Conceptualization, Methodology, Validation, Writing – review & editing, Supervision.

Acknowledgement

This work was supported by the National Natural Science Foundation of China (Grant No. NSFC 42075127 and 42375038), and the AI & AI for Science Project of Nanjing University.

References

Arking, A. and Childs, J. D.: Retrieval of Cloud Cover Parameters from Multispectral Satellite Images, J. Appl. Meteor. Climatol., 24, 322–334, doi:10.1175/1520-0450, 1985.

Bai, H., Zheng, Z., Zhang, Y., Huang, H., and Wang, L.: Comparison of Satellite-based $PM_{2.5}$ Estimation from Aerosol Optical Depth and Top-of-atmosphere Reflectance, Aerosol Air Qual. Res., 21, 1–17, doi:10.4209 /aaqr.2020.05.0257, 2021.

Delanoë, J., & Hogan, R. J.: Combined CloudSat-CALIPSO-MODIS retrievals of the properties of ice clouds. Journal of Geophysical Research: Atmospheres, 115(D4), doi:10.1029/2009JD012346, 2010.

Forster, P., T. Storelvmo, K. Armour, W. Collins, J.-L. Dufresne, D. Frame, D.J. Lunt, T. Mauritsen, M.D. Palmer, M. Watanabe, M. Wild, and H. Zhang: The Earth's Energy Budget, Climate Feedbacks, and Climate Sensitivity. In Climate Change 2021: The Physical Science Basis. Contribution of Working Group I to the Sixth Assessment Report of the Intergovernmental Panel on Climate Change [Masson-Delmotte, V., P. Zhai, A. Pirani, S.L. Connors, C. Péan, S. Berger, N. Caud, Y. Chen, L. Goldfarb, M.I. Gomis, M. Huang, K. Leitzell, E. Lonnoy, J.B.R. Matthews, T.K. Maycock, T. Waterfield, O. Yelekçi, R. Yu, and B. Zhou (eds.)]. Cambridge University Press, Cambridge, United Kingdom and New York, NY, USA, pp. 923–1054, doi:10.1017/9781009157896.009, 2021.

Garrett, K. J., Yang, P., Nasiri, S. L., Yost, C. R., & Baum, B. A.: Influence of cloud-top height and geometric thickness on a MODIS infrared-based ice cloud retrieval. Journal of applied meteorology and climatology, 48(4), 818-832, doi:10.1175/2008JAMC1915.1, 2009.

Guo, C., Ai, W., Hu, S., Du, X., & Chen, N.: Sea surface wind direction retrieval based on convolution neural network and wavelet analysis, IEEE Journal of Selected Topics in Applied Earth Observations and Remote Sensing, 15, 3868-3876, doi:10.1109/JSTARS.2022.3173001, 2022.

Häkansson, N., Adok, C., Thoss, A., Scheirer, R., and Hörnquist, S.: Neural network cloud top pressure and height for MODIS, Atmos. Meas. Tech., 11, 3177–3196, doi:10.5194/AMT-11-3177-2018, 2018.

Hamada, A. and Nishi, N.: Development of a cloud-top height estimation method by geostationary satellite split-window measurements trained with cloudsat data, J. Appl. Meteorol. Climatol., 49, 2035–2049, doi:10.1175/2010JAMC2287.1, 2010.

515   Han Yong, Paul van Delst, Quanhua Liu, Fuzhong Weng, Banghua Yan, Russ Treadon, and J. D.: JCSDA Community Radiative Transfer Model (CRTM): Version 1, NOAA Technical Report NESDIS, 122, 2006.

Harshvardhan, Zhao, G., Di Girolamo, L., and Green, R. N.: Satellite-observed location of stratocumulus cloud-top heights in the presence of strong inversions, IEEE Transactions on Geoscience and Remote Sensing, 47, 1421–1428, doi:10.1109/TGRS.2008.2005406, 2009.

520   Hersbach, H., Bell, B., Berrisford, P., Hirahara, S., Horányi, A., Muñoz Sabater, J., Nicolas, J., Peubey, C., Radu, R., Schepers, D., Simmons, A., Soci, C., Abdalla, S., Abellan, X., Balsamo, G., Bechtold, P., Biavati, G., Bidlot, J., Bonavita, M., De Chiara, G., Dahlgren, P., Dee, D., Diamantakis, M., Dragani, R., Flemming, J., Forbes, R., Fuentes, M., Geer, A., Haimberger, L., Healy, S., Hogan, R. J., Hólm, E., Janisková, M., Keeley, S., Laloyaux, P., Lopez, P., Lupu, C., Radnoti, G., de Rosnay, P., Rozum, I.,

525   Vamborg, F., Villaume, S., and Thépaut, J.-N.: The ERA5 global reanalysis, Q. J. Roy. Meteor. Soc., 146, 1999–2049, doi:10.1002/qj.3803, 2020.

Hong, G., Yang, P., Huang, H. L., Baum, B. A., Hu, Y., & Platnick, S.: The sensitivity of ice cloud optical and microphysical passive satellite retrievals to cloud geometrical thickness, IEEE transactions on geoscience and remote sensing, 45(5), 1315-1323, doi:10.1109/TGRS.2007.894549 ,2007.

530   Inoue, Toshiro: On the temperature and effective emissivity determination of semi-transparent cirrus clouds by bi-spectral measurements in the 10μm window region, Journal of the Meteorological Society of Japan. Ser. II 63.1: 88-99, doi:10.2151/jmsj1965.63.1_88, 1985.

Iwabuchi, H., PUTRI, N. S., SAITO, M., TOKORO, Y., SEKIGUCHI, M., YANG, P., and BAUM, B. A.: Cloud Property Retrieval from Multiband Infrared Measurements by Himawari-8, Journal of the

535   Meteorological Society of Japan. Ser. II, 96B, 27–42, doi:10.2151/jmsj.2018-001, 2018.

Iwabuchi, H., Saito, M., Tokoro, Y., Putri, N. S., & Sekiguchi, M.: Retrieval of radiative and microphysical properties of clouds from multispectral infrared measurements, Progress in Earth and Planetary Science, 3, 1-18, doi:10.1186/s40645-016-0108-3, 2016.

Lai, R., Teng, S., Yi, B., Letu, H., Min, M., Tang, S., and Liu, C.: Comparison of cloud properties from Himawari-8 and FengYun-4A geostationary satellite radiometers with MODIS cloud retrievals, Remote Sens., 11,1703, doi:10.3390/rs11141703, 2019.

Li, D., Saito, M., Yang, P., Loeb, N. G., Smith, W. L., & Minnis, P.: On the Scattering-Angle Dependence of the Spectral Consistency of Ice Cloud Optical Thickness Retrievals Based on Geostationary Satellite Observations, IEEE Transactions on Geoscience and Remote Sensing, 61, 1-12, doi:10.1109/TGRS.2023.3331970, 2023.

Libois, Q., & Blanchet, J. P.: Added value of far-infrared radiometry for remote sensing of ice clouds, Journal of Geophysical Research: Atmospheres, 122(12), 6541-6564, doi:10.1002/2016JD026423, 2017.

Liou, K. N. and Davies, R.: Radiation and Cloud Processes in the Atmosphere, Phys Today, 46, 66–67, doi:10.1063/1.2809044, 1993.

Marchand, R., Mace, G. G., Ackerman, T., and Stephens, G.: Hydrometeor detection using Cloudsat - An earth-orbiting 94-GHz cloud radar, J. Atmos. Oceanic Technol., 25, 519–533, doi:10.1175/2007JTECHA1006.1, 2008.

Menzel, W. P., Smith, W. L., & Stewart, T. R.: Improved cloud motion wind vector and altitude assignment using VAS, Journal of Applied Meteorology and Climatology, 22(3), 377-384, doi: 10.1175/1520-0450(1983)022<0377:ICMWVA>2.0.CO;2, 1983.

Menzel, W. P., Frey, R. A., Zhang, H., Wylie, D. P., Moeller, C. C., Holz, R. E., Maddux, B., Baum, B. A., Strabala, K. I., & Gumley, L. E.: MODIS global cloud-top pressure and amount estimation: Algorithm description and results, Journal of Applied Meteorology and Climatology, 47(4), 1175-1198, doi:10.1175/2007JAMC1705.1, 2008

Min, M., Li, J., Wang, F., Liu, Z., and Menzel, W. P.: Retrieval of cloud top properties from advanced geostationary satellite imager measurements based on machine learning algorithms, Remote Sens., Environ., 239, 111616, doi:10.1016/j.rse.2019.111616, 2020.

Minnis, P., Sun-Mack, S., Young, D. F., Heck, P. W., Garber, D. P., Chen, Y., ... & Yang, P.: CERES edition-2 cloud property retrievals using TRMM VIRS and Terra and Aqua MODIS data—Part I: Algorithms, IEEE Transactions on Geoscience and Remote Sensing, 49(11), 4374-4400, doi: 10.1109/TGRS.2011.2144601, 2011.

Nakajima, T., and M. D. King: Determination of the Optical Thickness and Effective Particle Radius of Clouds from Reflected Solar Radiation Measurements. Part I: Theory, J. Atmos. Sci., 47, 1878–1893, doi:10.1175/1520-0469, 1990

570

Painemal, D. and Zuidema, P.: Assessment of MODIS cloud effective radius and optical thickness retrievals over the Southeast Pacific with VOCALS-REx in situ measurements, Journal of Geophysical Research Atmospheres, 116, 1–16, doi:10.1029/2011JD016155, 2011.

Pilewskie, P., & Twomey, S.: Cloud phase discrimination by reflectance measurements near 1.6 and 2.2

575   µm, Journal of the atmospheric sciences, 44(22), 3419-3420, doi:10.1175/1520-0469(1987)044<3419:CPDBRM>2.0.CO;2, 1987.

Poulsen, C. A., Siddans, R., Thomas, G. E., Sayer, A. M., Grainger, R. G., Campmany, E., Dean, S. M., Arnold, C., and Watts, P. D.: Cloud retrievals from satellite data using optimal estimation: Evaluation and application to ATSR, Atmos. Meas. Tech., 5, 1889–1910, doi:10.5194/AMT-5-1889-2012, 2012.

580   Rodgers, C. D.: Inverse methods for atmospheric sounding: theory and practice, Vol.2., World scientific, 2000.

Rossow, W. B., L. C. Garder, and A. A. Lacis.: Global, Seasonal Cloud Variations from Satellite Radiance Measurements. Part I: Sensitivity of Analysis, J. Climate, **2**, 419–458, doi:10.1175/1520-0442, 1989.

Sassen, K., Wang, L., Starr, D. O., Comstock, J. M., and Quante, M.: A midlatitude cirrus cloud

585   climatology from the facility for atmospheric remote sensing. Part V: Cloud structural properties, J. Atmos. Sci., 64, 2483–2501, doi:10.1175/JAS3949.1, 2007.

Sassen, K., Wang, Z., and Liu, D.: Global distribution of cirrus clouds from CloudSat/cloud-aerosol lidar and infrared pathfinder satellite observations (CALIPSO) measurements, Journal of Geophysical Research Atmospheres, 114, 1–12, doi:10.1029/2008JD009972, 2009.

590   Shi, C., Hashimoto, M., Shiomi, K., & Nakajima, T.:Development of an algorithm to retrieve aerosol optical properties over water using an artificial neural network radiative transfer scheme: First result from GOSAT-2/CAI-2, IEEE Transactions on Geoscience and Remote Sensing, 59(12), 9861-9872, doi:10.1109/TGRS.2020.3038892, 2020.

Smith, W. L., Woolf, H. M., Abel, P., Hayden, C. M., Chalfant, M. W., & Grody, N. C.: NIMBUS-5

595   sounder data processing system, part I: measurement characteristics and data reduction procedures, NOAA technical memorandum NESS ; 57,1974.

Stubenrauch, C. J., A. Chédin, G. Rädel, N. A. Scott, and S. Serrar: Cloud properties and their seasonal and diurnal variability from TOVS Path-B, J. Climate, 19, 5531–5553, doi:10.1175/JCLI3929.1, 2006.

Tan, Z., Ma, S., Liu, C., Teng, S., Letu, H., Zhang, P., & Ai, W.: Retrieving cloud base height from passive

600   radiometer observations via a systematic effective cloud water content table. Remote Sensing of Environment, 294, 113633, doi:10.1016/j.rse.2023.113633, 2023.

Tan, Z., Ma, S., Liu, C., Teng, S., Xu, N., Hu, X., ... & Yan, W.: Assessing overlapping cloud top heights: An extrapolation method and its performance, IEEE Transactions on Geoscience and Remote Sensing, 60, 1-11, doi:10.1109/TGRS.2022.3170054, 2022.

605   Tana, G., Ri, X., Shi, C., Ma, R., Letu, H., Xu, J., and Shi, J.: Retrieval of cloud microphysical properties from Himawari-8/AHI infrared channels and its application in surface shortwave downward radiation estimation in the sun glint region, Remote Sens. Environ., 290, doi:10.1016/j.rse.2023.113548, 2023.

Twomey, S., and K. J. Seton: Inferences of gross microphysical properties of clouds from spectral reflectance measurements, J. Atmos. Sci., 37, 1065–1069, doi:10.1175/1520-0469, 1980.

610   Wang, C., Yang, P., Platnick, S., Heidinger, A. K., Baum, B. A., Greenwald, T., ... & Holz, R. E.: Retrieval of ice cloud properties from AIRS and MODIS observations based on a fast high-spectral-resolution radiative transfer model, Journal of applied meteorology and climatology, 52(3), 710-726, doi:10.1175/JAMC-D-12-020.1, 2013.

Wang, C., Platnick, S., Zhang, Z., Meyer, K., & Yang, P.: Retrieval of ice cloud properties using an

615   optimal estimation algorithm and MODIS infrared observations: 1. Forward model, error analysis, and information content, Journal of Geophysical Research: Atmospheres, 121(10), 5809-5826, doi:10.1002/2015JD024528, 2016.

Wang, C., Platnick, S., Zhang, Z., Meyer, K., Wind, G., & Yang, P.: Retrieval of ice cloud properties using an optimal estimation algorithm and MODIS infrared observations: 2. Retrieval evaluation, Journal

620   of Geophysical Research: Atmospheres, 121(10), 5827-5845, doi: 10.1002/2015JD024526, 2016.

Wang, J. and Christopher, S. A.: Intercomparison between satellite-derived aerosol optical thickness and $PM_{2.5}$ mass: Implications for air quality studies, Geophysical Research Letters, 30, 21, doi:10.1029/2003GL018174, 2003.

Wang, Q., Zhou, C., Zhuge, X., Liu, C., Weng, F., and Wang, M.: Retrieval of cloud properties from

625   thermal infrared radiometry using convolutional neural network, Remote Sens. Environ., 278, 113079,

doi:10.1016/j.rse.2022.113079, 2022.

Wang, Q., Zhou, C., Letu, H., Zhu, Y., Zhuge, X., Liu, C., Weng, F., and Wang, M.: Obtaining Cloud

Base Height and Phase from Thermal Infrared Radiometry Using a Deep Learning Algorithm, IEEE

Transactions on Geoscience and Remote Sensing, 61, doi:10.1109/TGRS.2023.3317532, 2023.

630   Yang, P., Tsay, S.-C., Wei, H., Guo, G., and Ji, Q.: Remote sensing of cirrus optical and microphysical

properties from ground-based infrared radiometric Measurements-part I: a new retrieval method based

on microwindow spectral signature, IEEE Geoscience and Remote Sensing Letters, 2, 128–131,

doi:10.1109/LGRS.2005.844733, 2005.

Yao, B., Liu, C., Yin, Y., Zhang, P., Min, M., & Han, W.: Radiance-based evaluation of WRF cloud

635   properties over East Asia: Direct comparison with FY-2E observations, Journal of Geophysical Research:

Atmospheres, 123(9), 4613-4629, doi:10.1029/2017JD027600, 2018.

Yi, B., Yang, P., Liu, Q., van Delst, P., Boukabara, S. A., & Weng, F.: Improvements on the ice cloud

modeling capabilities of the Community Radiative Transfer Model, Journal of Geophysical Research:

Atmospheres, 121(22), 13-577, doi:10.1002/2016JD025207, 2016.

640   Yuan, Q., Shen, H., Li, T., Li, Z., Li, S., Jiang, Y., Xu, H., Tan, W., Yang, Q., Wang, J., Gao, J., and Zhang,

L.: Deep learning in environmental remote sensing: Achievements and challenges, Remote Sensing of

Environment, 241, 111716, doi:10.1016/j.rse.2020.111716, 2020.

Zhang, Z., Yang, P., Kattawar, G., Riedi, J., -Labonnote, L. C., Baum, B. A., Platnick, S., and Huang, H.-

L.: Influence of ice particle model on satellite ice cloud retrieval: lessons learned from MODIS and

645   POLDER cloud product comparison, Atmos. Chem. Phys., 9, 7115–7129, doi:10.5194/acp-9-7115-2009,

2009.

Zhao, C., Xie, S., Klein, S. A., Protat, A., Shupe, M. D., McFarlane, S. A., Comstock, J. M., Delano, J.,

Deng, M., Dunn, M., Hogan, R. J., Huang, D., Jensen, M. P., MacE, G. G., McCoy, R., O'Connor, E. J.,

Turner, D. D., and Wang, Z.: Toward understanding of differences in current cloud retrievals of ARM

650   ground-based   measurements,   Journal   of   Geophysical   Research: Atmospheres,   117,

doi:10.1029/2011JD016792, 2012.

Zhao, Z., Zhang, F., Wu, Q., Li, Z., Tong, X., Li, J., & Han, W.: Cloud identification and properties retrieval of the Fengyun-4A satellite using a ResUnet model, IEEE Transactions on Geoscience and Remote Sensing, vol. 61, pp. 1–18, 2023, doi: 10.1109/TGRS.2023.3252023, 2023.

655 Zou, X., Zhuge, X., and Weng, F.: Characterization of bias of Advanced Himawari Imager infrared observations from NWP background simulations using CRTM and RTTOV, J. Atmos. Ocean Technol., 33, 2553–2567, doi:10.1175/JTECH-D-16-0105.1, 2016.